CMS Physics Analysis Summary

Contact: cms-pag-conveners-susy@cern.ch 2013/09/11

A search for anomalous production of events with three or more leptons using 19.5 fb^{-1} of $\sqrt{s}$=8 TeV LHC data

The CMS Collaboration

Abstract

A model-independent search for physics beyond the standard model in events with at least three leptons is presented. The data sample corresponds to 19.5 fb^{-1} of integrated luminosity in pp collisions at $\sqrt{s} = 8$ TeV collected by the CMS experiment at the LHC in 2012. Data is binned in exclusive channels characterized by lepton charge and flavor combinations, the magnitude of missing transverse energy and jet activity in the event, the invariant mass of opposite-sign lepton pairs consistent or inconsistent with decay of a Z boson, and the presence or absence of b-quarks and taus. The observations are consistent with expectations from standard model processes. We characterize the sensitivity of this analysis to new physics by interpreting the results in various supersymmetric models that yield multilepton final states including ones with Higgs bosons arising from supersymmetric decays. Finally, we place a 95% confidence level limit on the branching ratio for $t \to ch$ decays. We find that BR($t \to ch$) $< 0.31\%$, corresponding to a bound on the top-charm flavor violating Higgs Yukawa couplings of $\sqrt{|\lambda^h_{tc}|^2 + |\lambda^h_{ct}|^2} < 0.10$.

1 Introduction

Hadronic collisions yielding three or more electrons, muons, or taus (which define the "multi-lepton" signature) serve as an ideal final state to search for physics beyond the standard model (SM), as such final states are relatively rare in the SM but can be produced at high rates in new physics scenarios involving Electroweak processes or partner particles of gauge bosons and leptons [1].

In order to characterize the sensitivity of this analysis to possible new physics we use super-symmetry (SUSY) as a benchmark model. SUSY is a well regarded candidate for a beyond the standard model (BSM) theory because it solves the hierarchy problem, allows the unification of the gauge couplings, and may provide a candidate particle for dark matter [2–4].

A wide variety of SUSY scenarios yield events with multiple leptons. Below we describe three low scale SUSY/GMSB scenarios and two simplified model spectra (SMS) scenarios used to interpret these results [5, 6]. These scenarios encompass a range of coupling strengths, flavors, and intermediate particle identity, and are chosen to illustrate the reach of the analysis in different regimes.

Furthermore, we expoit the broad sensitivity of this analysis to set a limit on the flavor changing $t \to ch$ decay which – if observed – would provide evidence of new physics beyond the standard model. In the absence of statistically significant signal, the results can be used to set an upper bound on the top-charm flavor violating Higgs Yukawa couplings.

The exclusive final states are defined by lepton flavor, total hadronic energy in the event (H_T), $E_{\mathrm{T}}^{\mathrm{miss}}$ and the presence or absence of b-tagged jets. The search channels are coarsely divided in H_T and finely binned in $E_{\mathrm{T}}^{\mathrm{miss}}$. The events are further segregated according to the presence or absence of a leptonically decaying Z candidate as determined by the invariant mass of opposite-sign same-flavor (OSSF) pairs.

2 Data Samples and Event Selection

The data sample used in this analysis was recorded in 2012 with the CMS detector at the LHC and corresponds to an integrated luminosity of 19.5 fb^{-1}. The data used for the search has been collected using the double-lepton (double-electron, double-muon, muon-electron) triggers. The transverse momentum (p_T) cut-off for these triggers is 17 GeV for the leading lepton and 8 GeV for the next-to-leading lepton. The trigger efficiencies are measured directly using a data sample independently triggered by H_T, defined as the scalar sum of the transverse momentum of all jets with $p_T > 30\,\mathrm{GeV}$ and $|\eta| < 2.5$, assuming no correlations between these and the signal triggers. For events containing an electron or muon with $p_T > 20\,\mathrm{GeV}$, relevant for this analysis, the double-electron, double-muon, and muon-electron triggers efficiencies plateau at 95%, 90%, and 93% respectively. The double-muon trigger efficiency is essentially flat in p_T whereas double-electron and electron-muon cross trigger efficiencies show some p_T dependence. For $p_T < 20\,\mathrm{GeV}$ double electron trigger efficiency is 82% while the electron-muon cross trigger efficiency is 86%. We scale each simulated event by the probability for it to satisfy the double-lepton triggers. The uncertainty in the correction to the simulation translates into a systematic uncertainty in the irreducible backgrounds and signal efficiencies.

This analysis requires the presence of at least three reconstructed lepton candidates. The allowed candidates include electrons, muons and hadronically-decaying taus (τ_h); taus decaying leptonically (τ_ℓ) are included in the electron and muon counting. We use electrons and muons

with $p_T \geq 10\,\text{GeV}$ and $|\eta| < 2.4$. They are reconstructed using measured quantities from the tracker, calorimeter, and muon system using particle-flow (PF) algorithms [7]. The matching candidate tracks must satisfy quality requirements and spatially match with the energy deposits in the electromagnetic calorimeter and the tracks in the muon detectors, as appropriate. Details of reconstruction and identification can be found in Ref. [8] for electrons and in Ref. [9] for muons.

The hadronic tau decays predominantly yield either a single charged track (one-prong) or three charged tracks (three-prong) with or without additional electromagnetic energy from neutral pion decays as well as neutrinos. In this analysis, we use both one-prong and three-prong τ_h decays, reconstructed using the hadron plus strips (HPS) PF method [10]. We require the visible p_T of the τ to be greater than 20 GeV and $|\eta| \leq 2.3$.

We use PF isolation for our electrons and muons. An isolation requirement strongly reduces the background from misidentified leptons and leptons from the decays of heavy-flavor mesons, since most of them occur inside jets. We define the relative isolation I_{rel} as the ratio of the sum of the calorimeter energy and p_T of any other tracks in the cone defined by $\Delta R = \sqrt{(\Delta\eta)^2 + (\Delta\phi)^2} < 0.3$ around the lepton to the p_T of the lepton. For electrons and muons, we require $I_{\text{rel}} < 0.15$. The sum of energy in the isolation cone is corrected by subtracting out the expected contributions from additional vertices in the event. For the isolation of the hadronic tau decays we require that the sum in a cone of $\Delta R < 0.5$ is less than 2 GeV after subtracting the average expected contribution from additional overlapping pp interactions in the same and preceding bunch crossing. We use the same 0.02 cm cut for electrons and muons on the impact parameter (d_{xy}) between the track and the event vertex. We do not explicitly make a d_{xy} cut for taus but instead use recommended tau discriminants.

Only prompt leptons are selected in this analysis, as leptons in the theoretical models considered for the interpretation of the results originate from the interaction point. After the isolation selection, non-prompt leptons from heavy quark decays can be misidentified as prompt leptons, where the lepton tends to be more isolated because of the high p_T with respect to other visible particles within the jet. This background is reduced by requiring that the leptons originate from within half a centimeter of the primary vertex in z and that $d_{xy} \leq 0.02$ cm. The isolation and promptness criteria would retain the SUSY signal of prompt leptons, but restrict the background from misidentified leptons in the signal region. Although the fake leptons dominate the highly populated channels some of the more sensitive channels are dominated by diboson production. We reject events with $m(\ell^+\ell^-) < 12\,\text{GeV}$ in order to reject low mass Drell Yan and low mass resonances like J/ψ and Y. In order to remove leptons from conversions (internal and external) that arise from final state radiation from the Z daughters in the low-$E_{\text{T}}^{\text{miss}}$ and low-H_T region, we reject events, which satisfy both $|m(\ell^+\ell^-) - m_Z| > 15\,\text{GeV}$ and $|m(\ell^+\ell^-\ell'^{\pm}) - m_Z| < 15\,\text{GeV}$.

All detector simulations are performed using GEANT4 [11]. The important SM backgrounds for this analysis ($t\bar{t}$ quark pairs, and double vector boson production) were generated using MADGRAPH [12]. We use the CTEQ6.6 parton distribution functions [13]. For the dominant WZ+jets contribution up to two jets were selected at the matrix element level in MADGRAPH as the corresponding contributions are not negligible.

3 Search Strategy

Candidate events in this search must have at least three lepton candidates, where at most one of them is a hadronic τ candidate. The thresholds on the transverse momenta of the leptons are chosen such that triggers used are maximally efficient for selected events. Only electrons and muons are triggered on and the leading muon or electron is required to have $p_T > 20\,\text{GeV}$ while additional muons and electrons are required to have $p_T > 10\,\text{GeV}$. Taus are required to have visible $p_T > 20\,\text{GeV}$. We classify multilepton events into search channels on the basis of the number of leptons, lepton and jet flavor as well as charge and flavor combinations and other kinematic quantities described below.

We classify each event in terms of the maximum number of opposite-sign same flavor (OSSF) dilepton pairs that can be made by using each identified lepton candidate only once. We denote a lepton pair of different flavors as $\ell\ell'$, where ℓ indicates an electron or a muon. For example, both $\mu^+\mu^-\mu^-$ and $\mu^+\mu^-e^-$ type events are categorized as OSSF1, $\mu^+\mu^+e^-$ is OSSF0, and a $\mu^+\mu^-e^+e^-$ event is qualified as OSSF2. The level of the SM background varies considerably across the channels. Channels with hadronic tau decays or containing OSSF pairs suffer from larger background contamination compared to channels with OSSF0. To maximize the overall sensitivity of the search, all these charge combinations are considered as separate channels.

We further classify events as containing a leptonically-decaying Z if at least one OSSF pair has reconstructed invariant mass ($m_{\ell^+\ell^-}$) in the Z-mass window, i.e. $|m_{\ell^+\ell^-} - m_Z| < 15\,\text{GeV}$. Another criterion for background reduction is the "Z veto", in which the invariant mass of the OSSF lepton pairs is required to be outside the Z-mass window, i.e. $|m_{\ell^+\ell^-} - m_Z| > 15\,\text{GeV}$.

An event is considered to contain b-jets if at least one jet passes the b jet discriminant which uses the CMS "Combined Secondary Vertex algorithm" [14]. The discriminant has a tagging efficiency of 70% and a misidentification rate for light flavor jets less than 2% for the medium working point. We classify events according to the presence or absence of b-jets. Jets are reconstructed using particles with $|\eta| \leq 2.5$ via the PF algorithm [7] and we use the anti-k_T algorithm [15] with a distance parameter of 0.5.

Multilepton signatures benefit from relatively low SM background contamination, which can be further reduced by minimal requirements on either hadronic activity or missing energy above those typical for main SM background contributions. The presence of hadronic activity in an event is characterized by the variable H_T. Jets used for the H_T determination must be well separated from any identified leptons and this is enforced by requiring no isolated leptons in a cone $\Delta R < 0.3$ around the jet axis. In this search, we classify events as having H_T greater or less than 200 GeV.

The missing transverse energy, E_T^miss, is defined as the magnitude of the vector sum of the momenta of all particle candidates reconstructed with the CMS Particle Flow [7] algorithm. Comparison between data and simulation shows good modeling of E_T^miss for processes with genuine E_T^miss from invisible neutrinos [16, 17]. In this search, the E_T^miss is divided into four 50 GeV wide bins from 0 to 200 GeV and a fifth bin containing events with $E_\text{T}^\text{miss} \geq 200\,\text{GeV}$.

4 Background Estimation

4.1 Background from Non-prompt Leptons or Tau Candidates

The largest background remaining after the requirement of at least three-lepton candidates originates from Z-boson production with associated jets, in which the Z boson decays leptonically and a third lepton is a result of misidentification from a jet in the event. This background dominates the lower $E_{\mathrm{T}}^{\mathrm{miss}}$ and H_T channels. Higher $E_{\mathrm{T}}^{\mathrm{miss}}$ and H_T cut suppress the component that originates from the Z+jets. Since the QCD component of the simulation cannot be deemed reliable as such misidentifications happen when rare fluctuations occur in jet fragmentation, we use data to estimate background contributions from processes with two genuine leptons and one or more misidentified leptons such as $Z(\to 2\ell) + \text{jets}$ and $W^+W^-(\to 2\ell) + \text{jets}$, known as the Drell-Yan production.

To estimate the rate of background contamination from processes with two genuine leptons and a misidentified lepton, we use data with two reconstructed leptons and an additional isolated track scaled by a conversion factor between isolated tracks and selected lepton candidates from jets. This conversion factor is measured in control samples where no signal is expected to be present, such as in low-$E_{\mathrm{T}}^{\mathrm{miss}}$, low-$H_T$ samples. This method has also been used in previous analyses [18]. We measure the conversion factor between isolated tracks and muon (electron) candidates to be $0.6\% \pm 0.2\%$ ($0.7\% \pm 0.2\%$) in a data sample dominated by Z+jets and where the systematic uncertainties are one half of the difference between the rates measured in the $\mu^+\mu^-$+isolated track sample and the corresponding rates measured in e^+e^-+isolated track sample. Therefore, the number of isolated tracks in the control sample is multiplied by the conversion factor. For example, the contribution of the backgrounds with a misidentified third lepton is obtained by multiplying the number of isolated tracks in the sample with two leptons by this conversion factor. The rates are expected to vary with heavy quark content across the control samples. The variation is accounted for by determining the rate as a function of the impact parameter of non-isolated tracks in the data, as the impact parameter of tracks coming from heavy flavor decays is much larger as compared to tracks coming from pion and kaon decays.

For channels with τ_h, we loosen the isolation requirements to get a conversion factor between loose taus and isolated taus [18].

In particular, we extrapolate from the sideband distribution $6\,\mathrm{GeV} < I < 15\,\mathrm{GeV}$ to the signal distribution $I < 2\,\mathrm{GeV}$, where I is the sum of the contribution in a cone of radius 0.3 in $\Delta R = \sqrt{(\Delta\eta)^2 + (\Delta\phi)^2}$ around the τ_h candidate. The conversion factor, defined as the ratio of the number of tau candidates in the signal region to the number of tau candidates in the sideband region, is $(20 \pm 6)\%$. We study the variation of this ratio for a number of jet-dominated samples and assign a 30% systematic uncertainty for it. The ratio is multiplied by the number of events with 2ℓ+1 sideband τ.

4.2 Irreducible Background from WZ production

The SM can produce three or more genuine prompt leptons with $E_{\mathrm{T}}^{\mathrm{miss}}$ or H_T via diboson+jets production where both bosons decay leptonically. This type of background is referred to as "irreducible" because its characteristics are similar to the search signature and the expected rate of these events is obtained from theory and Monte Carlo simulations. The uncertainty of the theoretical cross section is 6%.

Again, we correct the simulation to match measured lepton efficiencies and $E_{\mathrm{T}}^{\mathrm{miss}}$ resolution

in the same way as was done for $t\bar{t}$. To correct the $E_{\mathrm{T}}^{\mathrm{miss}}$ resolution, we subdivide the $E_{\mathrm{T}}^{\mathrm{miss}}$ distribution as a function of the number of vertices and H_T in the event. A large number of vertices in an event indicates a larger extraneous energy in reconstructed objects due to pileup. This stochastic contribution results in worse $E_{\mathrm{T}}^{\mathrm{miss}}$ resolution.

On the other hand, a larger H_T indicates higher jet activity, leading to systematically larger tails in the $E_{\mathrm{T}}^{\mathrm{miss}}$ distribution due to mis-reconstruction. We model the $E_{\mathrm{T}}^{\mathrm{miss}}$ for events without real $E_{\mathrm{T}}^{\mathrm{miss}}$ (from neutrinos) as a sum of Rayleigh distributions given by

$$p(x) = \sum_{ij} W_{ij} \frac{x}{\sigma_{ij}^2} e^{-x^2/2\sigma_{ij}^2} \tag{1}$$

where "i" represents the number of vertices in the event and "j" indicates the H_T bin, and the weight W_{ij} is the fraction of events in the bin. Coefficients σ_{ij} are fitted for and characterize the $E_{\mathrm{T}}^{\mathrm{miss}}$ resolution in both dilepton data and the simulation. We then smear the $E_{\mathrm{T}}^{\mathrm{miss}}$ in simulation on an event by event basis to match the coefficients with data. The magnitude of the correction to the $E_{\mathrm{T}}^{\mathrm{miss}}$ in simulation samples due to the additional smearing varies from a few percent to as high as 25%. The systematic uncertainty is obtained by studying the migration of events due to the additional smearing.

The simulation is checked against control samples. We validate this procedure by comparing with data samples enriched in WZ-production, the dominant contribution to trilepton signatures from diboson+jets. WZ samples can be selected by requiring three leptons, $50\,\mathrm{GeV} < E_{\mathrm{T}}^{\mathrm{miss}} < 100\,\mathrm{GeV}$, and an on-shell Z i.e. an OSSF pair with the invariant mass satisfying $75\,\mathrm{GeV} < m_{\ell\ell} < 105\,\mathrm{GeV}$ and $H_T < 200\,\mathrm{GeV}$.

Figure 1 shows the $E_{\mathrm{T}}^{\mathrm{miss}}$ distribution in the WZ control region. These backgrounds are well modeled by the simulation.

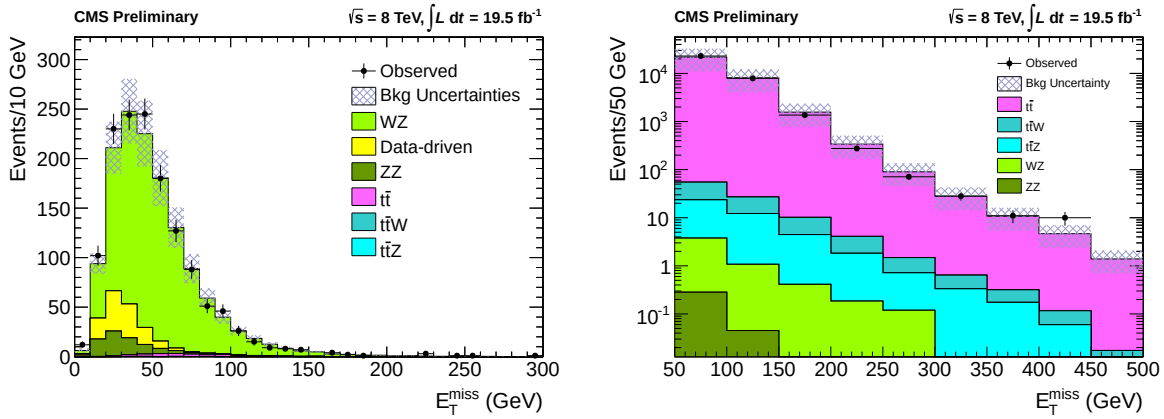

Figure 1: Distributions for $E_{\mathrm{T}}^{\mathrm{miss}}$ in the WZ and opposite sign $e\mu$ dilepton $t\bar{t}$ control regions.

4.3 Background from $t\bar{t}$ Production

This background contribution is estimated from simulation after careful validation in the single lepton and dilepton control regions enriched with $t\bar{t}$. We correct the simulation to match measured lepton efficiencies and the $E_{\mathrm{T}}^{\mathrm{miss}}$ resolution. The single lepton control region requires one isolated muon with $p_T > 30\,\mathrm{GeV}$, at least three jets, one of which must satisfy a medium

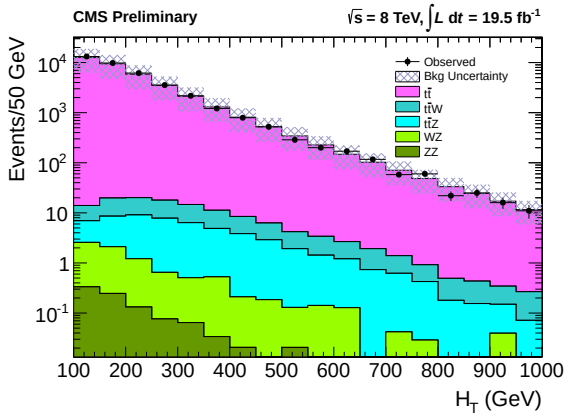

Figure 2: Distribution for H_T in the opposite sign $e\mu$ dilepton $t\bar{t}$ control region.

b-tagging working point, and the sum of H_T, $E_{\mathrm{T}}^{\mathrm{miss}}$, and all selected lepton p_T (S_T) $> 300\,\mathrm{GeV}$, and is used to study the relative isolation distribution of non-prompt lepton from b-jets. The dilepton control region requires an opposite-sign $e\mu$ pair and is used to compare kinematical variables like S_T, H_T, and $E_{\mathrm{T}}^{\mathrm{miss}}$ between data and simulation. In addition, the distribution of the number of jets is reweighted to match data in the dilepton control region. We observed good agreement in the kinematic variables S_T, H_T, and $E_{\mathrm{T}}^{\mathrm{miss}}$, and we apply a correction factor for the isolation distribution of leptons from jets. Figures 1 and 2 show the $E_{\mathrm{T}}^{\mathrm{miss}}$ and H_T distributions for the opposite sign $e\mu$ dilepton $t\bar{t}$ control region, respectively.

4.4 Backgrounds from Asymmetric Internal Photon Conversions

There are two different types of photon conversions that can give rise to backgrounds in multilepton analyses. The first type is an "external conversion" of an on-shell photon into an $\ell^+\ell^-$ pair in the material of the detector. This conversion is predominantly into e^+e^- pairs. The second type of photon conversions are "internal conversions" where the photon is virtual and can produce muons almost as often as electrons. In case of asymmetric conversions, where one lepton has very low p_T and does not pass the selection criteria, Drell-Yan processes with such conversions can lead to a significant background for three lepton signatures.

Simulation cannot be relied upon to evaluate this background correctly, since the soft lepton p_T is often below the generator-level p_T thresholds. Data-based measurements of the photon to e/μ conversion factors provide an estimate of asymmetric photon conversion backgrounds.

We measure the conversion factors in a control region where new physics is suppressed (low $E_{\mathrm{T}}^{\mathrm{miss}}$ and low H_T). The ratio of the number of events with $|m(\ell^+\ell^-\ell'^{\pm}) - m_Z| < 15\,\mathrm{GeV}$ or $|m(\ell^+\ell^-\ell^{\pm}) - m_Z| < 15\,\mathrm{GeV}$ to the number of events with $|m(\ell^+\ell^-\gamma) - m_Z| < 15\,\mathrm{GeV}$ defines the conversion factor, which is $0.7\% \pm 0.1\%$ ($2.0\% \pm 0.3\%$) for muons (electrons) [18]. The uncertainties are statistical only. We assign systematic uncertainties of 50% to these conversion factors from our underlying assumption of proportionality between virtual and on-shell photons. The measured conversion factors are then used to estimate the background in the signal regions from the observed number of $\ell^+\ell^-\gamma$ events in the signal regions. The background contribution from these converted photons is small after the final selection cuts, as will be shown in the next section.

5 Results and their Interpretation

Tables 1, 2, 3 and 4 show the expected and observed numbers of three- and four-lepton events after the $E_{\mathrm{T}}^{\mathrm{miss}}$ and H_T requirements. Categorization of events into separate channels used in the fitting procedure uses finer $E_{\mathrm{T}}^{\mathrm{miss}}$ binning. The channels have been combined into coarse $E_{\mathrm{T}}^{\mathrm{miss}}$ bins to make the table more succinct.

Tables 1, 2, 3 and 4 also show the observations and SM backgrounds in additional control regions, namely the non-signal regions with $E_{\mathrm{T}}^{\mathrm{miss}} < 50\,\mathrm{GeV}$ and/or $H_T < 200\,\mathrm{GeV}$ combined with or without a Z candidate in the event. Furthermore, the channels are classified according to the number of τ candidates as well as the number of b-jets (columns) which shows the larger background for events including hadronic τ decay candidates and no b-jets.

The observed number of events in the channels we examine is largely consistent with expectations.

Selection		$E_{\mathrm{T}}^{\mathrm{miss}}$	N(τ_{h})=0, $N_{\mathrm{b-jets}}$=0		N(τ_{h})=1, $N_{\mathrm{b-jets}}$=0		N(τ_{h})=0, $N_{\mathrm{b-jets}}\geq$1		N(τ_{h})=1, $N_{\mathrm{b-jets}}\geq$1	
4 Lepton Results			obs	exp	obs	exp	obs	exp	obs	exp
OSSF0 $H_T > 200$	NA	(100,∞)	0	0.01 ± 0.03	0	0.01 ± 0.06	0	0.02 ± 0.04	0	0.11 ± 0.08
OSSF0 $H_T > 200$	NA	(50,100)	0	$0.0^{+0.02}_{-0.00}$	0	0.01 ± 0.06	0	$0.0^{+0.03}_{-0.00}$	0	0.12 ± 0.07
OSSF0 $H_T > 200$	NA	(0,50)	0	1e-05 $\pm$ 0.02	0	0.07 ± 0.1	0	$0.0^{+0.02}_{-0.00}$	0	0.02 ± 0.02
OSSF1 $H_T > 200$	off-Z	(100,∞)	0	0.005 ± 0.02	1	0.25 ± 0.11	0	0.13 ± 0.08	0	0.12 ± 0.12
OSSF1 $H_T > 200$	on-Z	(100,∞)	1	0.1 ± 0.06	0	0.5 ± 0.27	0	0.42 ± 0.22	0	0.42 ± 0.19
OSSF1 $H_T > 200$	off-Z	(50,100)	0	0.07 ± 0.06	1	0.29 ± 0.13	0	0.04 ± 0.04	0	0.23 ± 0.13
OSSF1 $H_T > 200$	on-Z	(50,100)	0	0.23 ± 0.11	1	0.7 ± 0.31	0	0.23 ± 0.13	1	0.34 ± 0.16
OSSF1 $H_T > 200$	off-Z	(0,50)	0	0.02 ± 0.03	0	0.27 ± 0.12	0	0.03 ± 0.04	0	0.31 ± 0.15
OSSF1 $H_T > 200$	on-Z	(0,50)	0	0.2 ± 0.08	0	1.3 ± 0.47	0	0.06 ± 0.04	1	0.49 ± 0.19
OSSF2 $H_T > 200$	off-Z	(100,∞)	0	0.01 ± 0.02	-	-	0	0.01 ± 0.06	-	-
OSSF2 $H_T > 200$	on-Z	(100,∞)	1	0.15 ± 0.16	-	-	0	0.34 ± 0.18	-	-
OSSF2 $H_T > 200$	off-Z	(50,100)	0	0.03 ± 0.02	-	-	0	0.13 ± 0.09	-	-
OSSF2 $H_T > 200$	on-Z	(50,100)	0	0.8 ± 0.4	-	-	0	0.36 ± 0.19	-	-
OSSF2 $H_T > 200$	off-Z	(0,50)	1	0.27 ± 0.13	-	-	0	0.08 ± 0.05	-	-
OSSF2 $H_T > 200$	on-Z	(0,50)	5	7.4 ± 3.5	-	-	2	0.8 ± 0.4	-	-

Table 1: A comparison of the number of observed events with the background expectation for 19.5 fb^{-1} of 2012 data. The labels going down the side refer to whether or not there are OSSF pairs, whether or not $Z \to \ell^+\ell^-$ was excluded (below-Z means $m_{ll} < 75\,\mathrm{GeV}$, above-Z means $m_{ll} > 105\,\mathrm{GeV}$, on-Z means m_{ll} between 75 and 105 GeV), and the H_T and $E_{\mathrm{T}}^{\mathrm{miss}}$ requirements. Labels along the top of the table give the number of τ_{h} candidates, 0 or 1 and the number of b-jets which is 0 or $\geq$1. All channels are exclusive. Note that the upper limits presented in this analysis have been obtained using channels defined with finer segmentation in $E_{\mathrm{T}}^{\mathrm{miss}}$.

5.1 Systematic Uncertainties and Statistical Procedures

We discuss the sources of systematic uncertainty on the signal acceptance times efficiency and how they impact the search sensitivity before extracting upper limits on the contributions from physics outside the SM. Table 5 lists the salient systematic effects and the resultant uncertainties. All channels share systematic uncertainties for luminosity, renormalization scales, parton distribution functions, and trigger efficiency. The precision in estimating lepton selection efficiencies increases with lepton p_T. For a typical slepton co-NLSP signal scenario which has leptons with p_T in excess of 20 GeV, the lepton identification and isolation efficiency systematic uncertainty is $\sim$ 1.5% per lepton. Overall, the total systematic uncertainties on the various signal channels vary between 3% and 40%, including lepton efficiency uncertainties, b-tag uncertainties, $E_{\mathrm{T}}^{\mathrm{miss}}$ uncertainties and the luminosity uncertainties. The ISR uncertainty is estimated by studying how the signal events migrate between the H_T bins when additional H_T

Selection 4 Lepton Results		$E_{\mathrm{T}}^{\mathrm{miss}}$	N(τ_{h})=0, $N_{\mathrm{b-jets}}$=0 obs	exp	N(τ_{h})=1, $N_{\mathrm{b-jets}}$=0 obs	exp	N(τ_{h})=0, $N_{\mathrm{b-jets}}\geq$1 obs	exp	N(τ_{h})=1, $N_{\mathrm{b-jets}}\geq$1 obs	exp
OSSF0 $H_T < 200$	NA	(100,∞)	0	0.11 ± 0.08	0	0.17 ± 0.1	0	0.03 ± 0.04	0	0.04 ± 0.04
OSSF0 $H_T < 200$	NA	(50,100)	0	0.01 ± 0.03	2	0.7 ± 0.33	0	$0.0^{+0.02}_{-0.00}$	0	0.28 ± 0.16
OSSF0 $H_T < 200$	NA	(0,50)	0	0.01 ± 0.02	1	0.7 ± 0.3	0	0.001 ± 0.02	0	0.13 ± 0.08
OSSF1 $H_T < 200$	off-Z	(100,∞)	0	0.06 ± 0.04	3	0.6 ± 0.24	0	0.02 ± 0.04	0	0.32 ± 0.2
OSSF1 $H_T < 200$	on-Z	(100,∞)	1	0.5 ± 0.18	2	2.5 ± 0.5	1	0.38 ± 0.2	0	0.21 ± 0.1
OSSF1 $H_T < 200$	off-Z	(50,100)	0	0.18 ± 0.06	4	2.1 ± 0.5	0	0.16 ± 0.08	1	0.45 ± 0.24
OSSF1 $H_T < 200$	on-Z	(50,100)	2	1.2 ± 0.34	9	9.6 ± 1.6	2	0.42 ± 0.23	0	0.5 ± 0.16
OSSF1 $H_T < 200$	off-Z	(0,50)	2	0.46 ± 0.18	15	7.5 ± 2	0	0.09 ± 0.06	0	0.7 ± 0.31
OSSF1 $H_T < 200$	on-Z	(0,50)	4	3 ± 0.8	41	40 ± 10	1	0.31 ± 0.15	2	1.5 ± 0.47
OSSF2 $H_T < 200$	off-Z	(100,∞)	0	0.04 ± 0.03	-	-	0	0.05 ± 0.04	-	-
OSSF2 $H_T < 200$	on-Z	(100,∞)	0	0.34 ± 0.15	-	-	0	0.46 ± 0.25	-	-
OSSF2 $H_T < 200$	off-Z	(50,100)	2	0.18 ± 0.13	-	-	0	0.02 ± 0.03	-	-
OSSF2 $H_T < 200$	on-Z	(50,100)	4	3.9 ± 2.5	-	-	0	0.5 ± 0.21	-	-
OSSF2 $H_T < 200$	off-Z	(0,50)	7	8.9 ± 2.4	-	-	1	0.23 ± 0.09	-	-
OSSF2 $H_T < 200$	on-Z	(0,50)	*156	159 ± 34	-	-	4	2.9 ± 0.8	-	-

Table 2: A comparison of the number of observed events with the background expectation for 19.5 fb^{-1} of 2012 data. The labels going down the side refer to whether or not there are OSSF pairs, whether or not $Z \to \ell^+\ell^-$ was excluded (below-Z means $m_{ll} < 75\,\mathrm{GeV}$, above-Z means $m_{ll} > 105\,\mathrm{GeV}$, on-Z means m_{ll} between 75 and 105 GeV), and the H_T and $E_{\mathrm{T}}^{\mathrm{miss}}$ requirements. Labels along the top of the table give the number of τ_{h} candidates, 0 or 1 and the number of b-jets which is 0 or $\geq$1. All channels are exclusive. Note that the upper limits presented in this analysis have been obtained using channels defined with finer segmentation in $E_{\mathrm{T}}^{\mathrm{miss}}$. Channels marked with an asterisk are used as control regions and are excluded from the limit calculations.

Selection 3 Lepton Results		$E_{\mathrm{T}}^{\mathrm{miss}}$	N(τ_{h})=0, $N_{\mathrm{b-jets}}$=0 obs	exp	N(τ_{h})=1, $N_{\mathrm{b-jets}}$=0 obs	exp	N(τ_{h})=0, $N_{\mathrm{b-jets}}\geq$1 obs	exp	N(τ_{h})=1, $N_{\mathrm{b-jets}}\geq$1 obs	exp
OSSF0 $H_T > 200$	NA	(100,∞)	5	3.7 ± 1.6	35	33 ± 14	1	5.5 ± 2.2	47	61 ± 30
OSSF0 $H_T > 200$	NA	(50,100)	3	3.5 ± 1.4	34	36 ± 16	8	7.7 ± 2.7	82	91 ± 46
OSSF0 $H_T > 200$	NA	(0,50)	4	2.1 ± 0.8	25	25 ± 9.7	1	3.6 ± 1.5	52	59 ± 29
OSSF1 $H_T > 200$	above-Z	(100,∞)	5	3.6 ± 1.2	2	10 ± 4.8	3	4.7 ± 1.6	19	22 ± 11
OSSF1 $H_T > 200$	below-Z	(100,∞)	7	9.7 ± 3.3	18	14 ± 6.4	8	9.1 ± 3.4	21	23 ± 11
OSSF1 $H_T > 200$	on-Z	(100,∞)	39	61 ± 23	17	15 ± 4.9	9	14 ± 4.4	10	12 ± 5.8
OSSF1 $H_T > 200$	above-Z	(50,100)	4	5 ± 1.6	14	11 ± 5.2	6	6.8 ± 2.4	32	30 ± 15
OSSF1 $H_T > 200$	below-Z	(50,100)	10	11 ± 3.8	24	19 ± 6.4	10	9.9 ± 3.7	25	32 ± 16
OSSF1 $H_T > 200$	on-Z	(50,100)	78	80 ± 32	70	50 ± 11	22	22 ± 6.3	36	24 ± 9.8
OSSF1 $H_T > 200$	above-Z	(0,50)	3	7.3 ± 2	41	33 ± 8.7	4	5.3 ± 1.5	15	23 ± 11
OSSF1 $H_T > 200$	below-Z	(0,50)	26	25 ± 6.8	110	86 ± 23	5	10 ± 2.5	24	26 ± 11
OSSF1 $H_T > 200$	on-Z	(0,50)	*135	127 ± 41	542	543 ± 159	31	32 ± 6.5	86	75 ± 19

Table 3: A comparison of the number of observed events with the background expectation for 19.5 fb^{-1} of 2012 data. The labels going down the side refer to whether or not there are OSSF pairs, whether or not $Z \to \ell^+\ell^-$ was excluded (below-Z means $m_{ll} < 75$ GeV, above-Z means $m_{ll} > 105$ GeV, on-Z means m_{ll} between 75 and 105 GeV), and the H_T and $E_{\mathrm{T}}^{\mathrm{miss}}$ requirements. Labels along the top of the table give the number of τ_{h} candidates, 0 or 1 and the number of b-jets which is 0 or $\geq$1. All channels are exclusive. Note that the upper limits presented in this analysis have been obtained using channels defined with finer segmentation in $E_{\mathrm{T}}^{\mathrm{miss}}$. Channels marked with an asterisk are used as control regions and are excluded from the limit calculations.

due to initial state radiation is injected. We take this additional H_T distribution from a dataset where the jets are expected to originate from ISR. The associated uncertainty ranges between 0 % and 10 % depending on the mass point and channel under consideration. Cross section

Selection 3 Lepton Results		$E_{\mathrm{T}}^{\mathrm{miss}}$	N(τ_{h})=0, $N_{\mathrm{b-jets}}$=0 obs	exp	N(τ_{h})=1, $N_{\mathrm{b-jets}}$=0 obs	exp	N(τ_{h})=0, $N_{\mathrm{b-jets}}\geq$1 obs	exp	N(τ_{h})=1, $N_{\mathrm{b-jets}}\geq$1 obs	exp
OSSF0 $H_T < 200$	NA	(100,∞)	7	11 ± 4.9	101	111 ± 54	13	10 ± 5.3	87	119 ± 61
OSSF0 $H_T < 200$	NA	(50,100)	35	38 ± 15	406	402 ± 152	29	26 ± 13	269	298 ± 151
OSSF0 $H_T < 200$	NA	(0,50)	53	51 ± 11	910	1035 ± 255	29	23 ± 10	237	240 ± 113
OSSF1 $H_T < 200$	above-Z	(100,∞)	18	13 ± 3.5	25	38 ± 18	10	6.5 ± 2.9	24	35 ± 18
OSSF1 $H_T < 200$	below-Z	(100,∞)	21	24 ± 9	41	50 ± 25	14	20 ± 10	42	54 ± 28
OSSF1 $H_T < 200$	on-Z	(100,∞)l	150	152 ± 26	39	48 ± 13	15	14 ± 4.8	19	23 ± 11
OSSF1 $H_T < 200$	above-Z	(50,100)	50	46 ± 9.7	169	139 ± 48	20	18 ± 8	85	93 ± 47
OSSF1 $H_T < 200$	below-Z	(50,100)	142	125 ± 27	353	355 ± 92	48	48 ± 23	140	133 ± 68
OSSF1 $H_T < 200$	on-Z	(50,100)	*773	777 ± 116	1276	1154 ± 306	56	47 ± 13	81	75 ± 32
OSSF1 $H_T < 200$	above-Z	(0,50)	178	196 ± 35	1676	1882 ± 540	17	18 ± 6.7	115	94 ± 42
OSSF1 $H_T < 200$	below-Z	(0,50)	510	547 ± 87	9939	8980 ± 2660	34	42 ± 11	226	228 ± 63
OSSF1 $H_T < 200$	on-Z	(0,50)	*3869	4105 ± 666	*50188	50162 ± 14984	*148	156 ± 24	906	925 ± 263

Table 4: A comparison of the number of observed events with the background expectation for 19.5 fb^{-1} of 2012 data. The labels going down the side refer to whether or not there are OSSF pairs, whether or not $Z \to \ell^+\ell^-$ was excluded (below-Z means $m_{ll} < 75\,\mathrm{GeV}$, above-Z means $m_{ll} > 105\,\mathrm{GeV}$, on-Z means m_{ll} between 75 and 105 GeV), and the H_T and $E_{\mathrm{T}}^{\mathrm{miss}}$ requirements. Labels along the top of the table give the number of τ_{h} candidates, 0 or 1 and the number of b-jets which is 0 or $\geq$1. All channels are exclusive. Note that the upper limits presented in this analysis have been obtained using channels defined with finer segmentation in $E_{\mathrm{T}}^{\mathrm{miss}}$. Channels marked with an asterisk are used as control regions and are excluded from the limit calculations.

uncertainties are treated separately based on the uncertainties provided with their calculation.

Source of Uncertainty	Uncertainty
Luminosity	4.4%
PDF	14%
Renormalization Scale	10%
$E_{\mathrm{T}}^{\mathrm{miss}}$ Resolution/Smearing: $0-50\,\mathrm{GeV}, 50-100\,\mathrm{GeV}, >100\,\mathrm{GeV}$	(-3%, +4%, +4%)
Jet Energy Scale $W^{\pm}Z$	0.5% (WZ)
B-Tag Veto	0.1% (WZ), 6% ($t\bar{t}$)
Muon ID/Isolation at 10 (100) GeV	11% (0.2%)
Electron ID/Isolation at 10 (100) GeV	14% (0.6%)
Tau ID/Isolation at 10 (100) GeV	2% (1.1%)
$t\bar{t}$ cross-section/fake rate	50%
WZ normalization	6%
ZZ normalization	12%
Internal conversion fake rate	100%

Table 5: The systematic uncertainties associated with this analysis. The $E_{\mathrm{T}}^{\mathrm{miss}}$ resolution systematic is given for WZ background on Z for different cuts on $E_{\mathrm{T}}^{\mathrm{miss}}$ and for different cuts on M_T given a cut of $E_{\mathrm{T}}^{\mathrm{miss}} > 50\,\mathrm{GeV}$.

To calculate limits on signal parameters and cross sections, we divide the channels shown in Tables 1, 2, 3 and 4 by lepton flavor and perform a counting experiment using the observed event yields, the background expectations, and the signal expectations as inputs. We combine the limits from the channels with the highest individual expected sensitivities, which we require in aggregate to contain at least 90% of the signal acceptance at the relevant model grid point [18]. We use the LHC-type $\mathrm{CL_s}$ method in the limit calculation [19–22]. We use log-normal nuisance

parameters for the signal- and background-estimate uncertainties.

We set 95% confidence level (C.L.) upper limits on the signal parameters and cross sections using the modified frequentist construction (usually referred to as CLs) [20–22] with the LHC-style test statistic.

6 Benchmark Supersymmetric Scenarios

SUSY is a suitable model to represent new physics with multiple leptons. Multilepton final states can arise in several SUSY scenarios. We demonstrate the sensitivity of this search in the context of five benchmark MSSM scenarios involving superpartners of the leptons (sleptons, staus), bottom quark (sbottom), and top quark (stop).

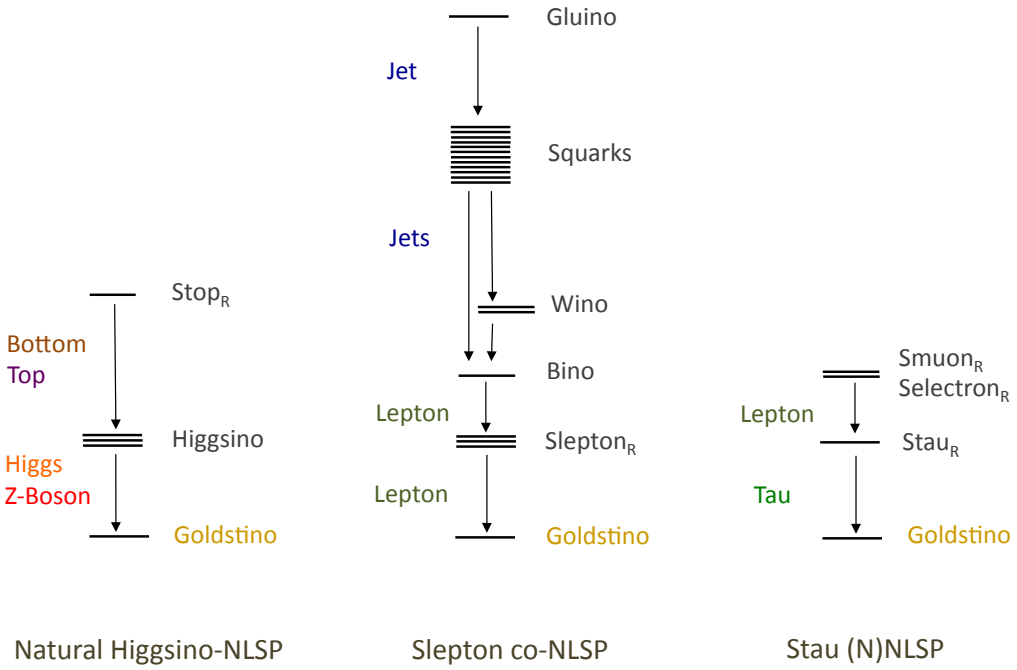

Figure 3: Mass spectra for the GMSB scenarios.

The first three scenarios which will be presented feature the gravitino as the lightest supersymmetric particle (LSP) that escapes the detector, but differ greatly in the strength of production mechanism. The fourth and fifth scenarios proceed through production of partners of third generation quarks, and yield final states enriched with heavy flavor and multiple leptons.

The natural SUSY Higgsino next-to-lightest supersymmetric particle (NLSP) scenario includes stop squark production with cascade decays to a neutral di-boson pair that can include one or two Higgs bosons, and missing energy [23]. Depending on the mass choices, the slepton co-NLSP model can produce squarks and gluinos with relatively large cross sections as well as weakly interacting particles, which then decay to multiple leptons and large missing transverse energy ($E_{\mathrm{T}}^{\mathrm{miss}}$). At the other extreme of relatively low cross section, the stau-NLSP proceeds through electroweak production of right-handed sleptons, and yields two τ leptons and relatively soft leptons or vice versa. Together, these two scenarios span a range of sensitivities

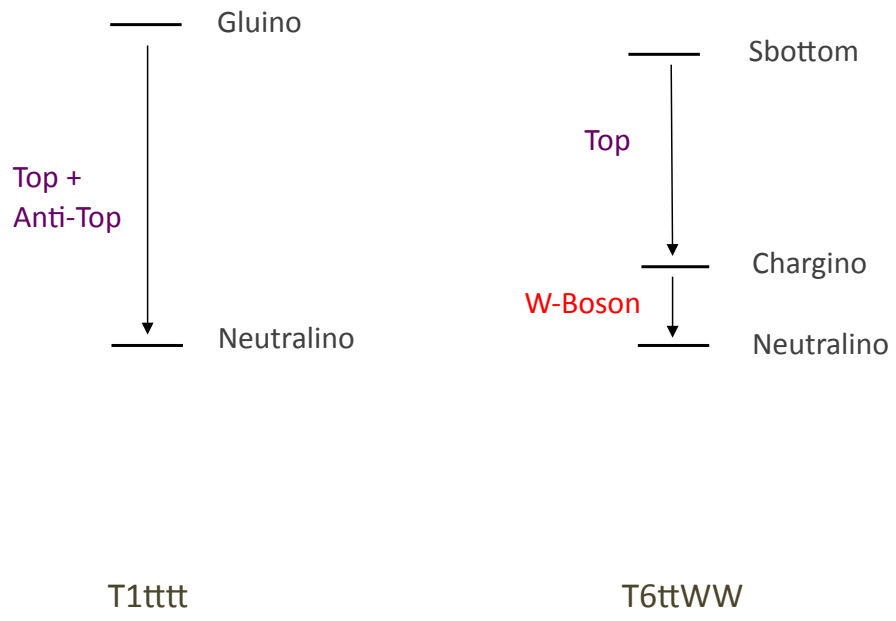

Figure 4: Mass spectra for the SMS scenarios.

to new physics production and decay topologies. Scenarios such as slepton co-NLSP have a high cross section with little background while scenarios like stau-(N)NLSP with their small production cross section present a more challenging multilepton signature.

The T1tttt and T6ttWW models both with 100% branching ratio proceed through third generation superpartners, and have neutralinos as the LSP in the final state. The T1tttt features gluino pair production, which decay to four top quarks, leading to multiple b-quarks, leptons and $E_{\mathrm{T}}^{\mathrm{miss}}$ in the final state. The T6ttWW features direct sbottom pair production, which decay to two top quarks and two W bosons. Together, the two scenarios show the reach of the multilepton analysis in new physics models with heavy flavor final states. The mass spectra and Feynman diagrams for the various scenarios are given in Figs. 3, 4, and 5.

In summary, the slepton co-NLSP model populates the high-$E_{\mathrm{T}}^{\mathrm{miss}}$ and 3 and 4 lepton channels and depending on the mass spectrum it may or may not populate the high-H_T region, while the stau-NLSP and stau-NNLSP populate the channels with taus and large-$E_{\mathrm{T}}^{\mathrm{miss}}$. The T1tttt and T6ttWW populate the channels with b-tagged jets and the former prefers the high-H_T channels. The natural Higgsino NLSP scenario, on the other hand, has the distinct feature that the signal is more widely spread out over the search channels than any of the other four scenarios, including both on- and off-Z channels, depending on what the higgsino decays to.

Signal events for the slepton co-NLSP, stau-(N)NLSP, T1tttt, and T6ttWW scenarios were made using PYTHIA [24], a leading order (LO) generator, while signal events for the Natural Higgsino NLSP scenario were made using MADGRAPH with showering of the events done in PYTHIA. For the Natural Higgsino NLSP scenario private cross sections for the strong and electroweak production are used with a 20% theory uncertainty. Similarly, for the slepton co-NLSP and stau-(N)NLSP scenarios we use private cross sections with a flat 30% theory uncertainty. The cross sections were advanced to next-to-leading order (NLO) using k-factors from PROSPINO [25]. Official cross sections and their corresponding theory uncertainties are applied on the T1tttt

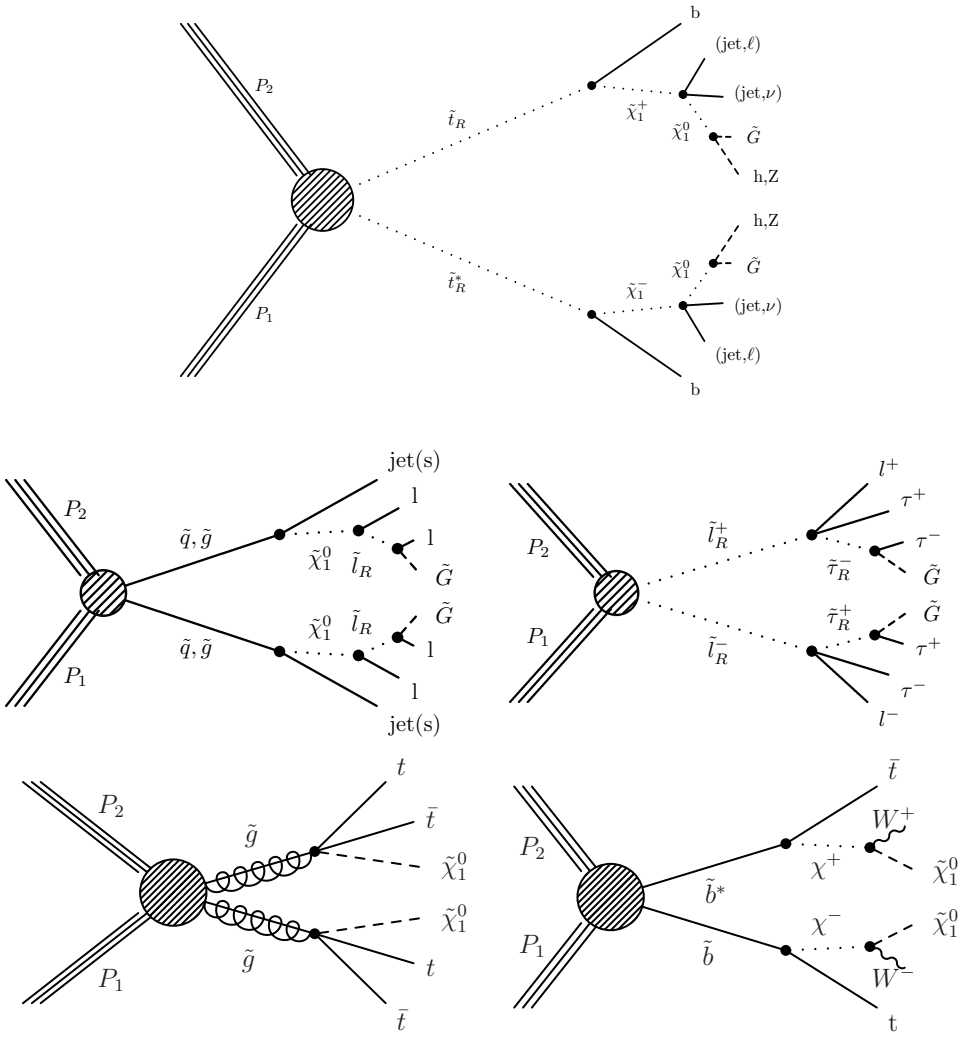

Figure 5: Diagrams for decays in the natural Higgsino NLSP scenario (top center), where the particles in parentheses are soft, the slepton co-NLSP scenario (middle left), the stau-NLSP scenario (middle right), the T1tttt scenario (bottom left), and the T6ttWW scenario (bottom right).

scenario [26]. As for the T6ttWW scenario, the official cross sections are used [27] with a flat 30% theory uncertainty.

6.1 Exclusion in the Natural Higgsino NLSP Scenario

We first present a natural Higgsino scenario. Production proceeds through right-handed stop–anti-stop pairs (strong production) with cascade decays

$$\widetilde{t}_R \to b\widetilde{\chi}_1^+,\ t\widetilde{\chi}_i^0 \tag{2}$$

where $i = 1, 2$. The final decay in all cascades is

$$\widetilde{\chi}_1^0 \to h\widetilde{G} \text{ or } Z\widetilde{G} \tag{3}$$

yielding an hh, ZZ, or hZ pair and $E_{\mathrm{T}}^{\mathrm{miss}}$ from the $\widetilde{G}$. Figure 5 (top center) illustrates this process. We also include direct production of Higgsino pairs through electroweak processes. Therefore, the Goldstino, $\widetilde{G}$, is the LSP while the Higgsino is the next-to-lightest supersymmetric particle (NLSP) for this scenario.

This model is particularly interesting and challenging because of the many decay modes available to the Higgs boson. We consider 7 decay channels of hh, namely WW*WW*, ZZ*ZZ*, $\tau\tau\tau\tau$, WW*ZZ*, WW$\tau\tau$, ZZ*$\tau\tau$, and ZZ*b$\bar{\text{b}}$. These decays yield events with three or more leptons. The Higgsinos, $\widetilde{\chi}_1^0$ and $\widetilde{\chi}_2^0$, are 5 GeV below and above the chargino-Higgsino, $\widetilde{\chi}_1^{\pm}$, respectively, while the Goldstino, $\widetilde{G}$, is assumed to be massless.

Figure 6 shows the excluded regions in the parameter space of this model for several choices of branching ratios. Figure 7 shows our exclusions in the cross section times branching ratio plane for fixed chargino mass. These curves are one dimensional slices of the plots in figure 6. We have more exclusion power at lower chargino mass since the cross section is larger. The Higgs dominant mode has less exclusion power due to the absence of EWKinos decaying to Z bosons.

These effects are further demonstrated in our sliding branching ratio plots, figure 8. As we go up in the vertical axis, the exclusion gets worse, again, because the branching ratio to Z decreases, and we are left with pure Higgs production at the top of the figures.

6.2 Exclusion in the Slepton co-NLSP Scenario

In supersymmetry, multilepton final states arise naturally in GMSB with split messengers (GMSM) where the right-handed sleptons are flavor-degenerate and at the bottom of the minimal supersymmetric standard model (MSSM) mass spectrum. The Higgsinos are decoupled. Supersymmetric production proceeds mainly through pairs of squarks and/or gluinos. Figure 5 (middle left) shows the schematic of the production and decay mechanism for the slepton co-NLSP model. If $m_{\widetilde{g}}$ is moderately low, strong production dominates and arises through pairs of squarks and gluinos, with cascade decays to the lightest neutralino and jets.

If instead, the gaugino masses are low, production takes place through chargino-neutralino pairs, with cascade decays to the lightest neutralino. The relative importance of strong and weak production depends on the ratio of gluino and chargino masses. Starting from any production, all cascade decays of these states eventually pass sequentially through the lightest neutralino, which decays to a right-handed slepton and a lepton. Starting from pair production, these cascade decays lead to events with four or more hard leptons, jets, and missing energy. The slepton co-NLSP model conserves R-parity and contains gravitinos as the stable LSP. Scenarios of this type arise in a wide class of GMSM theories [28, 29] and can result in multilepton final states [5, 28–30]. The slepton co-NLSP scenario arises in the subset of the GMSM parameter space where the right-handed sleptons are flavor-degenerate.

The 95% C.L. exclusion limit for the slepton co-NLSP model is shown in Fig. 9 (left). The superpartner mass spectra for these benchmarks are parameterized by the masses for the lightest chargino, $\widetilde{\chi}_1^{\pm}$, and the gluino, $\widetilde{g}$. The remaining superpartner masses are chosen to be $m_{\widetilde{\ell}_R} = 0.3\ m_{\widetilde{\chi}_1^{\pm}}$, $m_{\widetilde{\chi}_1^0} = 0.5\ m_{\widetilde{\chi}_1^{\pm}}$, $m_{\widetilde{\ell}_L} = 0.8\ m_{\widetilde{\chi}_1^{\pm}}$, and $m_{\widetilde{q}} = 0.8\ m_{\widetilde{g}}$, with vanishing left-right mixing for the squarks and sleptons, and the Higgsinos decoupled. The exclusion curve in

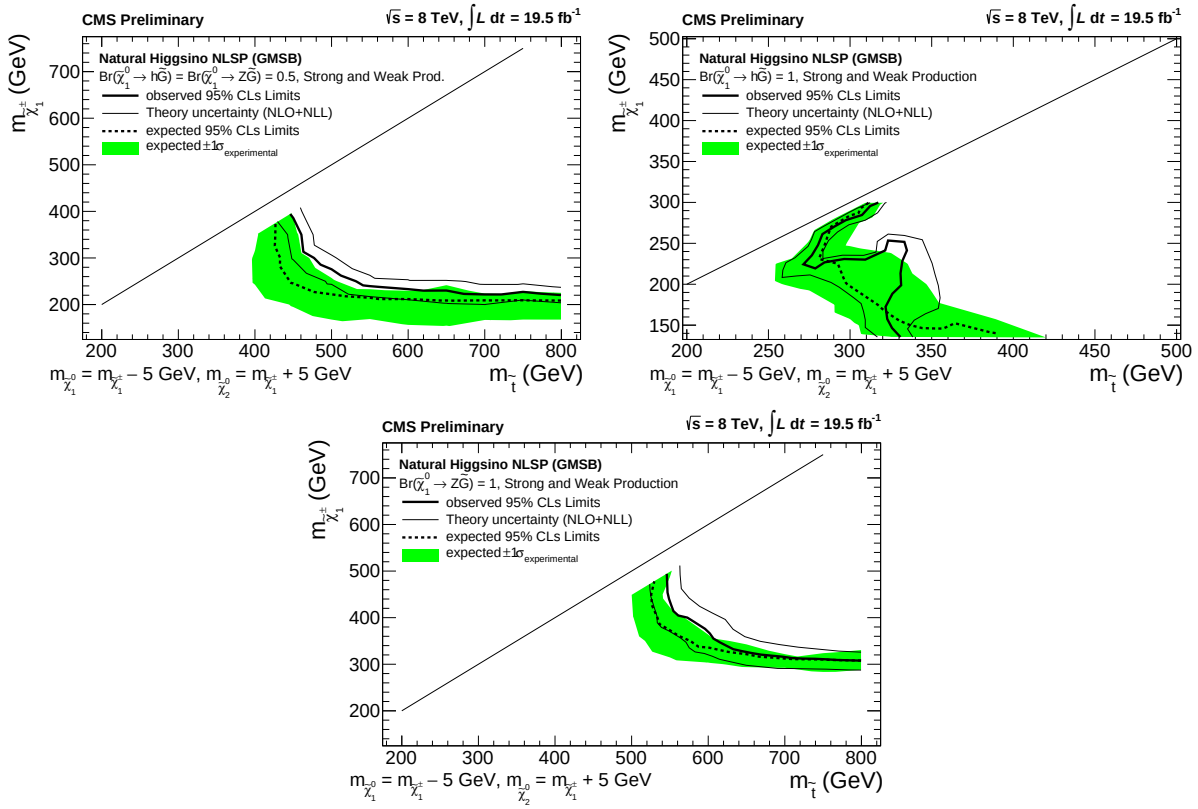

Figure 6: 95% C.L. limits for the natural Higgsino NLSP scenario with $\mathrm{Br}(\widetilde{\chi}_1^0 \to h\widetilde{G}) = \mathrm{Br}(\widetilde{\chi}_1^0 \to Z\widetilde{G}) = 0.5$ (top left), $\mathrm{Br}(\widetilde{\chi}_1^0 \to h\widetilde{G}) = 1.0$ (top right), and $\mathrm{Br}(\widetilde{\chi}_1^0 \to Z\widetilde{G}) = 1.0$ (bottom) for strong plus electroweak production. The region to the bottom left of the contours is excluded.

regions dominated by strong superpartner production tend to asymptotically approach a horizontal plateau while those dominated by weak superpartner production asymptotes towards the vertical. With strong superpartners decoupled, the production is dominated by wino-like chargino-neutralino and chargino-chargino production, as well as pair production of sleptons with lower masses that are set by the gauge ordered superpartner mass spectra.

6.3 Exclusion in the Stau-(N)NLSP Scenario

The stau-(N)NLSP model also conserves R-parity and contains gravitinos as the stable LSP. In this case, the sleptons are assumed to be NLSPs. The stau-NLSP scenario arises for moderate to large $\tan\beta$ where the right-handed stau is naturally lighter than the selectron or the smuon. In the stau-NLSP scenario the right-handed stau is lighter than the flavor degenerate right-handed smuon and selectron.

The selectron and smuon can then decay to the stau through the three-body decays

$$\widetilde{e}_R \to \widetilde{\tau}_R \tau e \qquad \widetilde{\mu}_R \to \widetilde{\tau}_R \tau \mu \tag{4}$$

The leptons that are emitted in these transition are relatively soft in the decay rest frame. The stau decays to a Goldstino and a tau

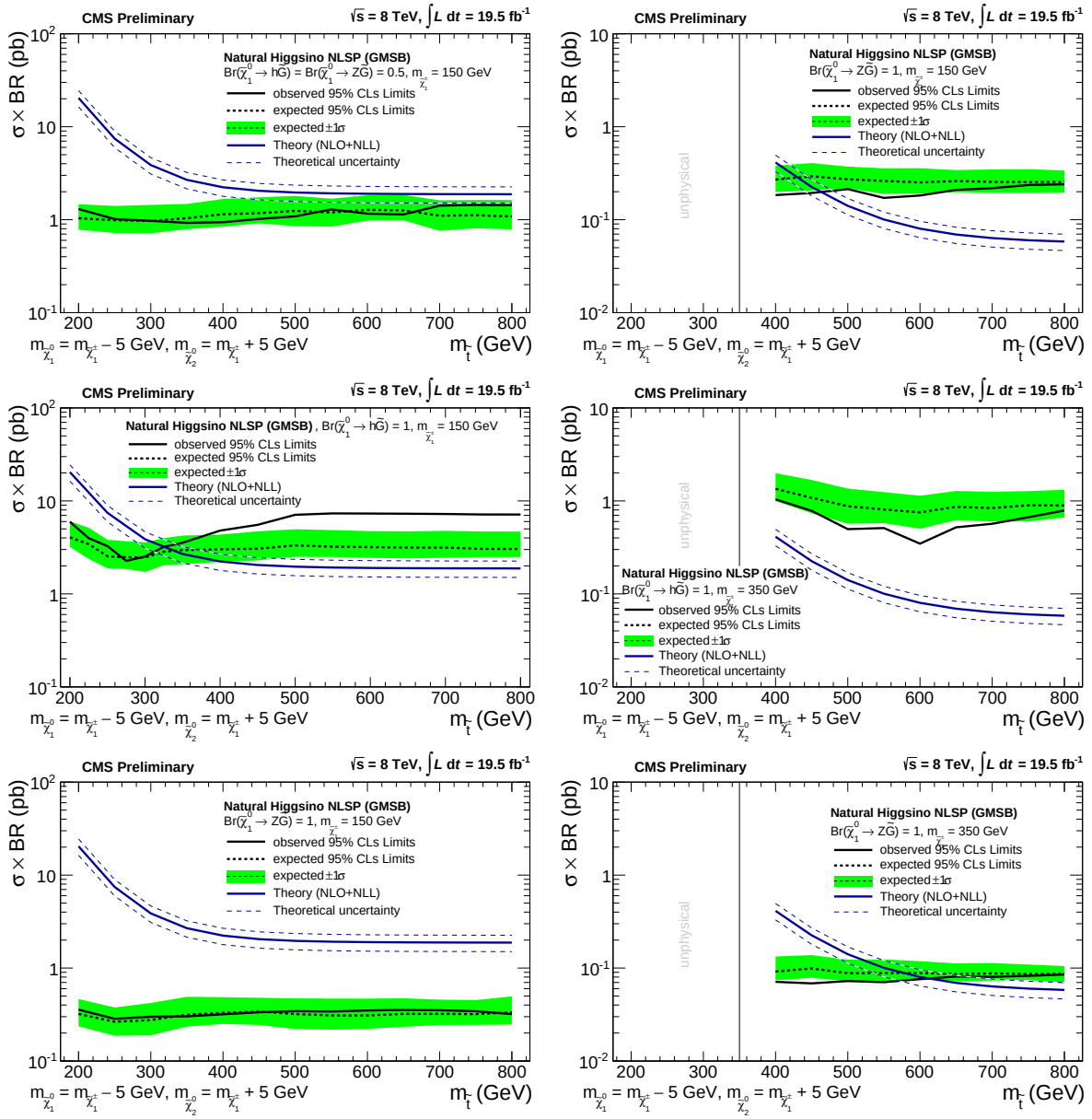

Figure 7: 95% C.L. limits for the natural Higgsino scenario with strong plus electroweak production for $\mathrm{Br}(\widetilde{\chi}_1^0 \to h\widetilde{G}) = \mathrm{Br}(\widetilde{\chi}_1^0 \to Z\widetilde{G}) = 0.5$ (top), $\mathrm{Br}(\widetilde{\chi}_1^0 \to h\widetilde{G}) = 1.0$ (middle), and $\mathrm{Br}(\widetilde{\chi}_1^0 \to Z\widetilde{G}) = 1.0$ (bottom). The chargino-Higgsino mass is fixed at 150 GeV (left) and 350 GeV (right). The region to the bottom left of the contours is excluded. The vertical line on the right illustrates the chargino-Higgsino mass; the space to the left of it is unphysical.

$$\widetilde{\tau}_R \to \widetilde{G}\tau \tag{5}$$

Figure 5 (middle right) illustrates this process. Starting from the weak pair production, these cascade decays then give rise to events with at least two taus, two other leptons, and missing energy (and additional soft leptons). We also consider the scenario wherein the right-handed stau is the next-to-next-to-lightest supersymmetric particle (NNLSP) and therefore heavier than

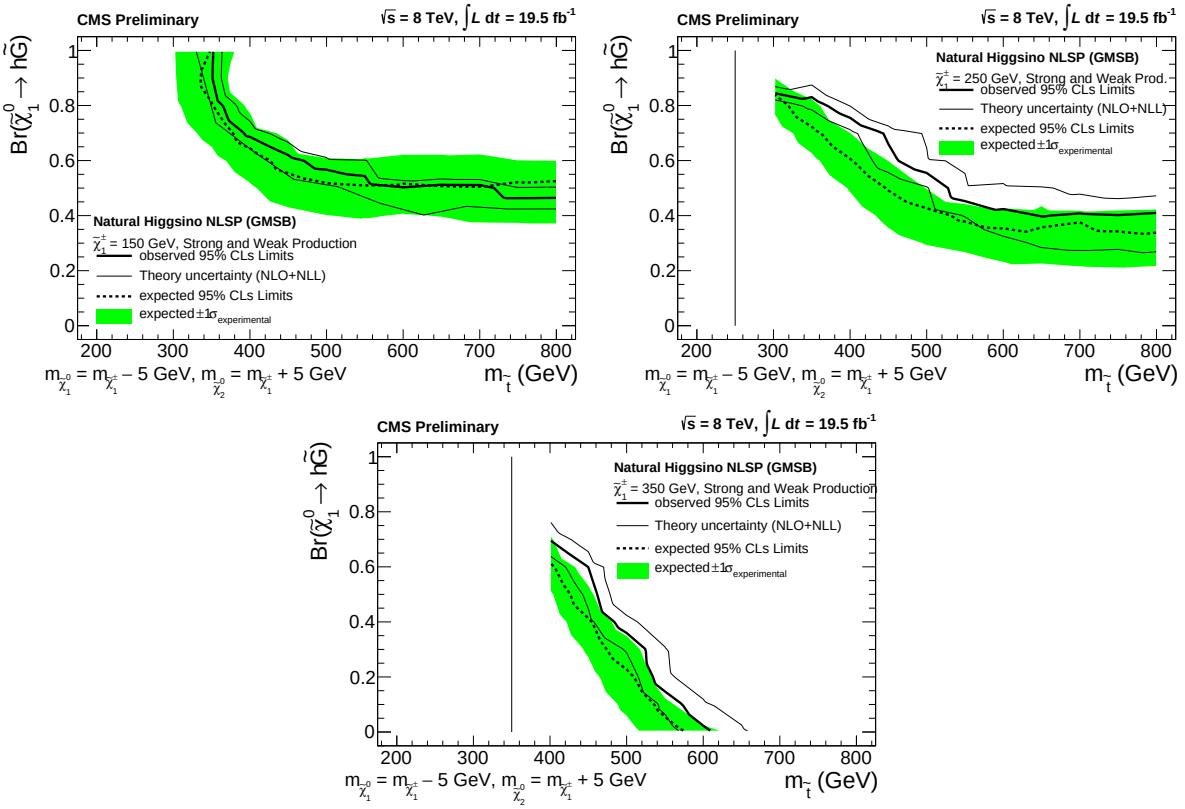

Figure 8: 95% C.L. limits on $\mathrm{Br}(\widetilde{\chi}_1^0 \to h\widetilde{G})$ for the natural Higgsino NLSP scenario with fixed chargino-Higgsino mass of 150 GeV (top left), 250 GeV (top right), and 350 GeV (bottom) assuming $\mathrm{Br}(\widetilde{\chi}_1^0 \to h\widetilde{G}) + \mathrm{Br}(\widetilde{\chi}_1^0 \to Z\widetilde{G}) = 1.0$ and strong plus weak production. The region to the bottom left of the contours is excluded. The vertical lines illustrate the chargino-Higgsino mass; the space to the left of them is unphysical.

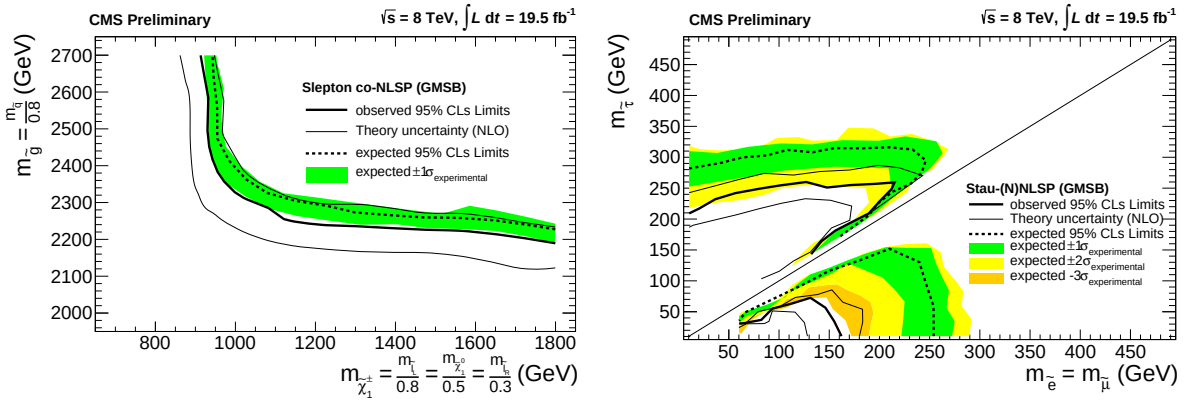

Figure 9: 95% C.L. limits for the slepton co-NLSP model in the gluino-chargino (wino-like chargino) mass plane (left) and for the stau-NLSP and stau-NNLSP scenario in the degenerate smuon- and selectron- stau mass plane (right) are shown. Masses to the left of the curve are excluded. The left figure shows 1σ and 2σ uncertainty bands while the right figure shows 1σ, 2σ, and 3σ uncertainty bands.

the mass degenerate right-handed smuon and selectron, which will then be the NLSPs. Both these scenarios in conjunction are referred to as the stau-(N)NLSP scenario.

The 95% C.L. exclusion limits for the stau-NLSP model is shown in Fig. 9 (right). When the mass difference between the stau and the other sleptons is small, the leptons become soft. This goes along with low signal efficiency which causes the exclusion contour to lie nearly parallel to the diagonal in that region of mass parameter space. The discrepancy between expected and observed 95% C.L. limits below the diagonal is driven by the $3(e/\mu)+\tau_h$ off Z channels with no b-tags and $H_T < 200\,\text{GeV}$. The three relevant entries in Table 2 refer to an observed (expected) yield of 15 (7.5 ± 2), 4 (2.1 ± 0.5), 3 (0.6 ± 0.24) events for the three different $E_{\text{T}}^{\text{miss}}$ bins. The probability of a statistical fluctuation in a single measurement with the expected yield of 10 ± 2.4 events to result in 22 or more observed events is only about 1%. However, once trial factors are incorporated to account for this analysis simultaneously looking at 64 individual channels, the probability of encountering as significant a fluctuation in the sum of the three $E_{\text{T}}^{\text{miss}}$ bins as observed in data is about 50%. Alternatively, the joint probability to observe as large an excess or larger for all three individual $E_{\text{T}}^{\text{miss}}$ bins in one of the 64 channels is about 5%. Correlated systematics are taken into account when evaluating these probabilities.

6.4 Exclusion in the 3rd Generation Scenario T1tttt

In the T1tttt scenario, the 3rd generation SUSY particles are produced via gluino-mediated stop production. This is one of many simplified benchmark models used at the LHC to cover an array of final states. We consider pair-production of gluinos where each gluino undergoes an effective three-body decay in the SMS approximation to $t\tilde{t}$. Each off-shell stop then decays to a $t\widetilde{\chi}_1^0$ resulting in a final state with four tops [31]. The tops can decay to give multileptonic final states.

In addition to frequently containing multiple leptons in the final state, these events also contain four b-tagged jets. The SM background can be significantly reduced by using b-tagging, a new feature of this analysis as compared to its previous version [18]. The main motivation for looking at this model is that a SUSY model with light particles, gluino in particular, solves the problem of fine-tuning of the Higgs mass. This is the first search to probe this signature in the multilepton final state.

This scenario is characterized by four top quarks in the final state, which results in four b-jets and four W bosons. In addition to producing four b-jets, this model produces large H_T and can produce up to four leptons with significant $E_{\text{T}}^{\text{miss}}$. Events with three and four leptons with large H_T, large $E_{\text{T}}^{\text{miss}}$, and multiple b-jets have little background.

The 95% C.L. exclusion limits in the $\widetilde{g} - \widetilde{\chi}_1^0$ mass plane are shown in Fig. 10 (left).

6.5 Exclusion in the 3rd Generation Scenario T6ttWW

In the T6ttWW scenario, we study possible SUSY signals with sbottom pair production. The bottom squark decaying as

$$\widetilde{b}_1 \to t\widetilde{\chi}_1^- \tag{6}$$

while the chargino decays as

$$\widetilde{\chi}_1^- \to W^-\widetilde{\chi}_1^0 \tag{7}$$

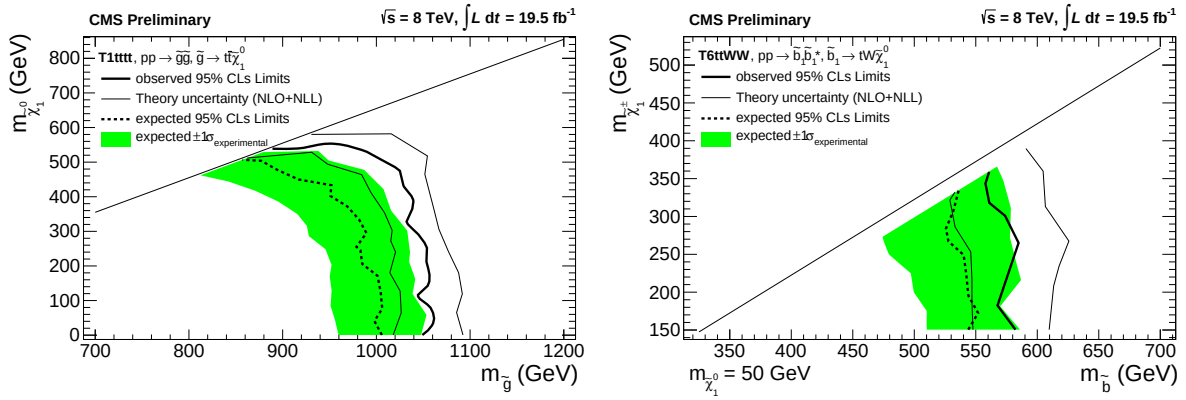

Figure 10: 95% C.L. limits for the T1tttt model in the gluino-neutralino mass plane (left) and for the T6ttWW model in the sbottom-chargino mass plane (right) are shown. Masses to the left of the curve which are below the diagonal are excluded. The figures show 1σ and 2σ uncertainty bands.

The production mechanisms for T6ttWW are shown in Fig. 5 (bottom right). The final states is then

$$t\bar{t}W^+W^-\widetilde{\chi}_1^0\widetilde{\chi}_1^0 \tag{8}$$

For simplicity we consider only mass parameters where the charginos are on-shell but the W from the chargino decay is allowed to be on- or off-shell. This scenario is an example of a "natural" SUSY which avoids excessive fine tuning [32].

Figure 10 (right) shows the exclusion for the T6ttWW scenario in the $\widetilde{b}_1 - \widetilde{\chi}_1^-$ mass plane. The mass of the $\widetilde{\chi}_1^0$ is assumed to be 50 GeV.

7 Limit on BR($t \to ch$)

We interpret the experimental results of this search in the context of the rare flavor-changing decay of the top quark to a Higgs boson and a charm quark. Although not forbidden in the standard model, the SM decay is suppressed both due to the Glashow-Iliopoulos-Maiani mechanism and second-third generation mixing [33]. Therefore, the SM branching ratio is quite small (10^{-13}–10^{-15}). Observation of $t \to ch$ at a higher rate would therefore provide evidence of new physics beyond the standard model.

Apart from that, this neutral flavor-changing decay can be used to directly probe flavor-violating couplings of the Higgs sector for the top quark, which has the largest coupling to the Higgs sector. Furthermore, since up-type quark flavor violation is less well constrained than down-type quark flavor violation, this process is of general experimental interest.

$t\bar{t}$ production followed by one of the top quarks decaying in this way can give multi-lepton final states, predominantly from the following Higgs decays:

- $h \to WW^* \to \ell\nu\ell\nu$,
- $h \to \tau\tau$,
- $h \to ZZ^* \to jj\ell\ell, \nu\nu\ell\ell, \ell\ell\ell\ell$.

If the other top quark in the $t\bar{t}$ pair undergoes $t \to bW$ with $W \to \ell\nu$ decay, up to five leptons can be produced.

For the generation of the signal, we simulated $t\bar{t}$ production events with one top quark decaying to Wb and the other decaying to ch. We assume $m_h = 125.5$ GeV with standard model branching ratios. The signal events were generated using MADGRAPH with the $t\bar{t}$ NNLO production cross-section $\sigma(pp \to t\bar{t}) = 245.8\,\text{pb}$ for 8 TeV [34].[1] The Higgs boson was decayed exclusively to the modes listed above. In total, we generated 500,000 events to ensure sufficient signal population in the multi-lepton channels used in this search.

We find that the signal predominantly populates channels that have three leptons (no hadronic tau), no OSSF pair or an OSSF pair off Z, and a b-tag. The the most sensitive channels are given in Table 6. No significant excess is observed.

OSSF pair	$E_{\text{T}}^{\text{miss}}$ [GeV]	H_T [GeV]	$N_{\text{b-tag}}$	data	background	signal
below Z	0–50	> 200	≥ 1	5	9.4 ± 2.6	12.3 ± 3.2
below Z	50–100	> 200	≥ 1	10	9.3 ± 3.6	12.7 ± 3.4
below Z	50–100	0–200	≥ 1	48	51 ± 25	39.5 ± 9.9
below Z	0–50	0–200	≥ 1	35	43 ± 12	23.9 ± 5.2
n/a	50–100	0–200	0	29	28 ± 14	21.8 ± 4.6
below Z	50–100	0–200	0	146	125 ± 29	41 ± 11
n/a	0–50	0–200	≥ 1	30	24 ± 11	16.1 ± 3.8
above Z	0–50	0–200	≥ 1	17	18.5 ± 6.7	10.8 ± 2.7
on Z	50–100	0–200	≥ 1	58	44 ± 13	16.0 ± 3.5
below Z	50–100	> 200	0	11	11.0 ± 3.8	7.1 ± 2.1

Table 6: The ten most sensitive signal regions for $t \to ch$ along with the number of observed, background, and expected signal events (assuming $\text{BR}(t \to ch) = 1\,\%$), ordered by sensitivity. All signal regions shown have exactly three selected leptons and no hadronic taus. The results are binned in $E_{\text{T}}^{\text{miss}}$, H_T, the presence of a b-tag, and – if applicable – the OSSF pair invariant mass with respect to the Z window.

Using the same procedure as for the other models, we obtain an observed limit of $\text{BR}_{95\,\%}^{\text{obs}}(t \to ch) = 0.31\,\%$ which corresponds to a bound on the top-charm flavor violating Higgs Yukawa couplings of $\sqrt{|\lambda_{tc}^h|^2 + |\lambda_{ct}^h|^2} < 0.10$. The expected limit is $\text{BR}_{95\,\%}^{\text{exp}}(t \to ch) = (0.31^{+0.15}_{-0.10})\,\%$. This is a significant improvement over the limit inferred in [33] from CMS multilepton results[18] with 5 fb^{-1} at 7 TeV.

To facilitate interpretation in a broader context [35], we also provide limits on $\text{BR}(t \to ch)$ from individual Higgs decay modes. For this purpose, we assume the SM branching ratio for the 125.5 GeV Higgs decay mode under consideration, and ignore other decay modes. Table 7 shows the results. This illustrates the sensitivity of this search for the $t \to ch$ decay in each of the Higgs decay modes.

[1] To obtain more conservative results, the cross-section was reduced by $1\sigma = 10.5$ pb. This applies to all results derived in this section.

Higgs Decay Mode	observed	expected	1σ range
$h \to WW$ (BR = 22.3 %)	0.37 %	0.38 %	(0.26–0.52) %
$h \to \tau\tau$ (BR = 6.24 %)	8.4 %	7.6 %	(5.8–11.2) %
$h \to ZZ$ (BR = 2.76 %)	1.23 %	0.97 %	(0.74–1.42) %
combined	0.31 %	0.31 %	(0.21–0.46) %

Table 7: Comparison of the observed and median expected 95% C.L. limits on BR($t \to ch$) from individual Higgs decay modes along with the 1σ uncertainty bands.

8 Conclusion

We have performed a search for physics beyond the SM using a variety of multilepton final states. We see good agreement between observations and expectations in channels with large SM expectations both on-Z and off-Z.

We used SUSY scenarios as benchmarks for new physics with multiple leptons. We were able to probe new regions of the natural Higgsino NLSP, slepton co-NLSP, stau-(N)NLSP, T1tttt, and T6ttWW scenarios. In the absence of any indication of new physics we place limits on supersymmetric mass spectra.

These models span a range of parameters, and the limits on intermediate and final state masses illustrate the reach of this analysis for most new physics scenarios with multiple leptons in the final state. Although we have chosen specific SUSY models to interpret our results, the masses and couplings from many other SUSY or non-supersymmetric new physics models can be translated into the framework of the models discussed here, and the limits applied to those models. The sensitivity of the analysis was further demonstrated by placing a limit on BR($t \to ch$).

References

[1] New Physics Working Group Collaboration, "New Physics at the LHC. A Les Houches Report: Physics at TeV Colliders 2009 - New Physics Working Group", arXiv:1005.1229.

[2] H. P. Nilles, "Supersymmetry, Supergravity and Particle Physics", *Phys. Rept.* **110** (1984) 1, doi:10.1016/0370-1573(84)90008-5.

[3] H. E. Haber and G. L. Kane, "The Search for Supersymmetry: Probing Physics Beyond the Standard Model", *Phys. Rept.* **117** (1985) 75, doi:10.1016/0370-1573(85)90051-1.

[4] W. de Boer, "Grand unified theories and supersymmetry in particle physics and cosmology", *Prog. Part. Nucl. Phys.* **33** (1994) 201, doi:10.1016/0146-6410(94)90045-0.

[5] LHC New Physics Working Group Collaboration, "Simplified Models for LHC New Physics Searches", *J.Phys.* **G39** (2012) 105005, doi:10.1088/0954-3899/39/10/105005, arXiv:1105.2838.

[6] J. K. R. Essig, E. Izaguirre et al., "Heavy Flavor Simplified Models at the LHC", *JHEP* **074** (2012) 1201, doi:10.1007/JHEPD01(2012)074.

[7] CMS Collaboration, "Commissioning of the Particle-Flow Reconstruction in Minimum-Bias and Jet Events from pp Collisions at 7 TeV", *CMS Physics Analysis Summary* **CMS-PAS-PFT-10-002** (2010).

[8] CMS Collaboration, "Electron Reconstruction and Identification at $\sqrt{s} = 7$ TeV", *CMS Physics Analysis Summary* **CMS-PAS-EGM-10-004** (2010).

[9] CMS Collaboration, "Performance of muon identification in pp collisions at $\sqrt{s} = 7$ TeV", *CMS Physics Analysis Summary* **CMS-PAS-MUO-10-002** (2010).

[10] CMS Collaboration, "Performance of τ-lepton reconstruction and identification in CMS", *JINST* **7** (2012), no. 01, P01001.

[11] GEANT4 Collaboration, "GEANT4: A simulation toolkit", *Nucl. Instrum. Meth.* **A506** (2003) 250, doi:10.1016/S0168-9002(03)01368-8.

[12] F. Maltoni and T. Stelzer, "MadEvent: Automatic event generation with MadGraph", *JHEP* **02** (2003) 027, doi:10.1088/1126-6708/2003/02/027.

[13] P. M. Nadolsky et al., "Implications of CTEQ global analysis for collider observables", *Phys. Rev.* **D78** (2008) 013004, doi:10.1103/PhysRevD.78.013004, arXiv:0802.0007.

[14] CMS Collaboration Collaboration, "Identification of b-quark jets with the CMS experiment", *JINST* **8** (2013) P04013, doi:10.1088/1748-0221/8/04/P04013, arXiv:1211.4462.

[15] M. Cacciari, G. P. Salam, and G. Soyez, "The anti-k_t jet clustering algorithm", *JHEP* **04** (2008) 063, doi:10.1088/1126-6708/2008/04/063, arXiv:0802.1189.

[16] CMS Collaboration, "Missing Transverse Energy Performance in Minimum-Bias and Jet Events from Proton-Proton Collisions at $\sqrt{s} = 7$ TeV", *CMS Physics Analysis Summary* **CMS-PAS-JME-10-004** (2010).

[17] CMS Collaboration, "CMS MET Performance in Events Containing Electroweak Bosons from pp Collisions at $\sqrt{s} = 7$ TeV", *CMS Physics Analysis Summary* **CMS-PAS-JME-10-005** (2010).

[18] CMS Collaboration, "Search for anomalous production of multilepton events in pp collisions at $\sqrt{s} = 7$ TeV", *JHEP* **1206** (2012) 169, doi:10.1007/JHEP06(2012)169, arXiv:1204.5341.

[19] ATLAS and CMS Collaboration, "Procedure for the LHC Higgs boson search combination in Summer 2011", Technical Report CMS-NOTE-2011-005, ATLAS/CMS, Geneva, (2011).

[20] T. Junk, "Confidence Level Computation for Combining Searches with Small Statistics", *Nucl. Instrum. Meth.* **A434** (1999) 435–443, doi:10.1016/S0168-9002(99)00498-2, arXiv:hep-ex/9902006.

[21] A. L. Read, "Modified frequentist analysis of search results (The CL(s) method)",. Prepared for Workshop on Confidence Limits, Geneva, Switzerland, 17-18 Jan 2000.

[22] A. L. Read, "Presentation of search results: The CL(s) technique", *J. Phys.* **G28** (2002) 2693–2704, doi:10.1088/0954-3899/28/10/313.

[23] K. T. Matchev and S. Thomas, "Higgs and Z-boson signatures of supersymmetry", *Phys. Rev. D* **62** (Sep, 2000) 077702, doi:10.1103/PhysRevD.62.077702.

[24] T. Sjöstrand, S. Mrenna, and P. Skands, "A Brief Introduction to PYTHIA 8.1", *Comput. Phys. Commun.* **178** (2008) 852, doi:10.1016/j.cpc.2008.01.036.

[25] W. Beenakker, R. Hopker, and M. Spira, "PROSPINO: A Program for the production of supersymmetric particles in next-to-leading order QCD", arXiv:hep-ph/9611232.

[26] CMS Collaboration, S. Padhi, "SUSYCrossSections8TeVgluglu". https://twiki.cern.ch/twiki/bin/view/LHCPhysics/SUSYCrossSections8TeVgluglu, 2013. [Online; accessed 01-September-2013].

[27] CMS Collaboration, S. Padhi, "SUSYCrossSections8TeVstopsbottom". https://twiki.cern.ch/twiki/bin/view/LHCPhysics/SUSYCrossSections8TeVstopsbottom, 2013. [Online; accessed 01-September-2013].

[28] S. Dimopoulos, S. D. Thomas, and J. D. Wells, "Implications of low energy supersymmetry breaking at the Fermilab Tevatron", *Phys. Rev.* **D54** (1996) 3283, doi:10.1103/PhysRevD.54.3283.

[29] SUSY Working Group Collaboration Collaboration, "Low scale and gauge mediated supersymmetry breaking at the Fermilab Tevatron Run II", arXiv:hep-ph/0008070. Physics at Run II SUSY/Higgs report: available as: fermilab-pub-00-349-1 (part 1), hep-ph/0003154 (part 2), hep-ph/0008070 (part 3), hep-ph/9906224 (part 4), hep-ph/0006162 (part 5), and hep-ph/0010338 (part 6).

[30] J. T. Ruderman and D. Shih, "Slepton co-NLSPs at the Tevatron", *JHEP* **1011** (2010) 046, doi:10.1007/JHEP11(2010)046, arXiv:1009.1665.

[31] CMS Collaboration Collaboration, "Interpretation of Searches for Supersymmetry with simplified Models", arXiv:1301.2175.

[32] H. M. Lee, V. Sanz, and M. Trott, "Hitting sbottom in natural SUSY", *JHEP* **1205** (2012) 139, doi:10.1007/JHEP05(2012)139, arXiv:1204.0802.

[33] N. Craig et al., "Searching for $t \to ch$ with multileptons", *Phys. Rev. D* **86** (Oct, 2012) 075002, doi:10.1103/PhysRevD.86.075002.

[34] M. Czakon, P. Fiedler, and A. Mitov, "The total top quark pair production cross-section at hadron colliders through $O(\alpha_S^4)$", 2013.

[35] K.-F. Chen, W.-S. Hou, C. Kao, and M. Kohda, "When the Higgs meets the Top: Search for $t \to ch^0$ at the LHC", arXiv:1304.8037.